UNIVERSITYOF BIRMINGHAM

Research at Birmingham

Insights into the Formation and Evolution of Individual Compounds in the Particulate Phase during Aromatic Photo-Oxidation

Pereira, Kelly L.; Hamilton, Jacqueline F.; Rickard, Andrew R.; Bloss, William; Alam, Mohammed; Camredon, Marie; Ward, Martyn W.; Wyche, Kevin P.; Muñoz, Amalia; Vera, Teresa; Vázquez, Mónica; Borrás, Esther; Ródenas, Milagros

Document Version
Peer reviewed version

Link to publication on Research at Birmingham portal

Article

Insights into the Formation and Evolution of Individual Compounds in the Particulate Phase during Aromatic Photo-oxidation

Kelly Louise Pereira, Jacqueline F Hamilton, Andrew Robert Rickard, William J. Bloss, Mohammed Salim Alam, Marie Camredon, Martyn W. Ward, Kevin P. Wyche, Amalia Munoz, Teresa Vera, Monica Vazquez, Esther Borras, and Milagros Ródenas

Just Accepted

Insights into the Formation and Evolution of Individual Compounds in the Particulate Phase during Aromatic Photo-oxidation

Kelly L. Pereira[1], Jacqueline F. Hamilton[1][*], Andrew R. Rickard[1,2], William. J. Bloss[3], Mohammed S. Alam[3], Marie Camredon[4], Martyn W. Ward[1], Kevin. P. Wyche[5], Amalia Muñoz[6], Teresa Vera[6], Mónica Vázquez[6], Esther Borrás[6], Milagros Ródenas[6].

[1]Wolfson Atmospheric Chemistry Laboratory, Department of Chemistry, University of York, York, UK. [2]National Centre for Atmospheric Science, University of York, UK. [3]School of Geography, Earth and Environmental Sciences, University of Birmingham, Birmingham, UK. [4]LISA, UMR CNRS/INSU 7583, University of Paris-Est Créteil and Paris Diderot, Créteil, France. [5]Air Environment Research, School Environment and Technology, University of Brighton, Brighton, UK. [6]CEAM-UMH, EUPHORE, Valencia, Spain.

[*]Corresponding author; e-mail: jacqui.hamilton@york.ac.uk. Phone: +44 (0)1904 324076. Fax: +44 (0) 1904 322516.

1

1 **Abstract**

2   Secondary organic aerosol (SOA) is well known to have adverse effects on air quality and

3   human health. However, the dynamic mechanisms occurring during SOA formation and

4   evolution are poorly understood. The time resolved SOA composition formed during the

5   photo-oxidation of three aromatic compounds, methyl chavicol, toluene and 4-methyl

6   catechol, were investigated at the European Photo-reactor. SOA was collected using a particle

7   into liquid sampler and analysed offline using state-of-the-art mass spectrometry to produce

8   temporal profiles of individual photo-oxidation products. In the photo-oxidation of methyl

9   chavicol, 70 individual compounds were characterised and three distinctive temporal profile

10 shapes were observed. The calculated mass fraction ($C_{i,\text{aer}}/C_{\text{OA}}$) of the individual SOA

11 compounds showed either a linear trend (increasing/decreasing) or exponential decay with

12 time. Substituted nitrophenols showed an exponential decay, with the nitro-group on the

13 aromatic ring found to control the formation and loss of these species in the aerosol phase.

14 Nitrophenols from both methyl chavicol and toluene photo-oxidation experiments showed a

15 strong relationship with the NO_2/NO (ppbv/ppbv) ratio and were observed during initial SOA

16 growth. The location of the nitrophenol aromatic substitutions was found to be critically

17 important, with the nitrophenol in the photo-oxidation of 4-methyl catechol not partitioning

18 into the aerosol phase until irradiation had stopped; highlighting the importance of studying

19 SOA formation and evolution at a molecular level.

20

21 **Introduction**

22   Secondary organic aerosol (SOA) constitutes a significant proportion of ambient particulate

23 matter[1-3] and exhibits substantial chemical complexity. The oxidation of a single volatile

24 organic compound (VOC) forms a wide variety of multi-functional products of differing

25 volatilities[4, 5]. These compounds may undergo numerous oxidation steps, forming a multitude

2

26   of oxidation products, only some of which may contribute to new particle formation and/or

27   SOA growth. Furthermore, once a compound partitions into the condensed phase it can

28   undergo further oxidation steps[6-9] and reactive transformations (non-oxidative processes, *i.e.*

29   oligomerisation)[10-15], resulting in continually changing chemical composition and volatility[4].

30   The sheer number of VOCs present in the ambient atmosphere[16] and their continually

31   evolving gas and particulate phase chemical composition, makes the identification of the

32   species involved in SOA formation, growth and ageing, a complex and difficult task. Recent

33   studies have found that extremely low volatility organic compounds (ELVOCs) can

34   participate in new particle formation and drive nanoparticle growth[17-23]; a topic which has

35   recently received considerable interest[2, 18, 24, 25]. Although, the detailed structural composition

36   of these ELVOCs have not been identified[23, 26].

37

38   Atmospheric simulation chambers can afford mechanistic insight into SOA formation

39   processes under simplified conditions. The oxidation of a single VOC precursor may be

40   investigated in a controlled environment, providing significant insight into the mechanisms

41   occurring during SOA formation and ageing. Bulk particle measurement techniques, such as

42   aerosol mass spectrometry and derivatives[27], provide near-real time chemical speciation of

43   non-refractory aerosol, allowing changes in particle oxidation to be observed[28, 29]. These

44   techniques have been invaluable to our understanding of the chemical and physical

45   transformations occurring during particle evolution. However, they cannot currently provide

46   the detailed chemical composition and structural speciation that offline mass spectrometric

47   techniques can offer[5, 30, 31].

48

49   Aromatic VOCs account for ~ 20 - 50 % of the non-methane hydrocarbon emissions in

50   urban areas[32, 33], with toluene often observed to be the most abundant species[33-35]. Aromatic

3

51   hydrocarbons are considered to be one of the most important SOA precursors, contributing

52   significantly to SOA formation[36-42]. Furthermore, their high reactivity makes them primary

53   contributors to photo-chemical ozone formation[43, 44]. However, despite their important impact

54   on urban air quality, aromatic photo-oxidation mechanisms are still poorly understood[45]. For

55   aromatic compounds such as alkyl-benzenes, typically emitted from gasoline sources, new

56   particle formation in chamber simulations has previously been shown to occur when the

57   experiment moves from RO_2 + NO dominated regime to a RO_2 + HO_2 or RO_2 regime[46-49],

58   suggesting that the species formed through this pathway are of sufficiently low volatility to

59   initiate nucleation[4, 47]. This has previously been attributed to the formation of peroxides,

60   although little compositional evidence has been found in aromatic systems to support this[23, 48]

61

62   SOA formation during the photo-oxidation of three mono-aromatic compounds, toluene (a

63   predominantly anthropogenic VOC), 4-methyl catechol (anthropogenic oxygenated-VOC,

64   OVOC) and methyl chavicol (biogenic OVOC, also known as estragole and 1-allyl-4-

65   methoxybenzene) were investigated at the European Photoreactor in Valencia, Spain. Sub-

66   micron aerosol samples were collected every 30 minutes using a particle into liquid sampler

67   (PILS) and analysed offline using; high performance liquid chromatography ion-trap mass

68   spectrometry (HPLC-ITMS), high performance liquid chromatography quadrupole time-of-

69   flight mass spectrometry (HPLC-QTOFMS) and Fourier transform ion cyclotron resonance

70   mass spectrometry (FTICR-MS). The use of a time resolved aerosol collection method

71   followed by offline state-of-the-art mass spectrometric analysis, has allowed us to provide

72   time resolved measurements with detailed chemical composition of the individual photo-

73   oxidation products formed. From this, we are able to observe the partitioning, formation and

74   loss of individual compounds in the particulate phase during SOA formation and ageing;

4

75   allowing us to observe the differences in the condensed phase evolution of individual species

76   based on their structure and functionality.

77

78   **Experimental**

79   **Chamber Simulation Experiments**

80   Experiments were performed at the European Photoreactor (EUPHORE) in Valencia,

81   Spain. Briefly, the EUPHORE facility consists of two ~ 200 m^3 hemispheric simulation

82   chambers made of fluorinated ethylene propylene foil (FEP). Dry scrubbed air is used within

83   the chamber and two large fans ensure homogenous mixing. Chamber temperature is near

84   ambient and pressure is maintained at ~ 100 Pa above ambient. Further technical information

85   can be found in the literature[45, 50-53]. Two sets of experiments were performed, during July

86   2009 as a part of the Toluene OXIdation in a Chamber (TOXIC) project and during May

87   2012 as a part of the Atmospheric Chemistry of Methyl Chavicol (ATMECH) project. VOC

88   precursors investigated, initial VOC/NO$_x$ mixing ratios and average chamber humidity and

89   temperature for the experiments discussed, are shown in Table 1.

90

91   The chamber was cleaned before each experiment by flushing with dry scrubbed air. The

92   VOC precursor was introduced into the chamber through a heated air stream. Photo-oxidation

93   experiments were performed, where no additional source of $^\bullet$OH radicals were added into the

94   chamber, using wall chemistry to initiate photo-oxidation[54, 55]. A range of instruments were

95   used to monitor chamber pressure (Barometer, model AIR-DB-VOC), humidity (Hygrometer

96   Watz, model Walz-TS2), temperature (temperature sensor, model PT100), solar intensity

97   (j(NO$_2$) Filter radiometer), NO$_x$ (Teledyne API, model NO$_X$_API-T200UP; photolytic

98   converter) and O$_3$ (Monitor Labs, model 9810). During the TOXIC project, precursor

99   degradation and product formation was monitored using a Fourier transform infra red

5

100   spectrometer (FTIR, Nicolet Magna, model 550) coupled to a white-type mirror system

101   (optical path length 616 m) and a chemical ionisation reaction time-of-flight mass

102   spectrometer (CIR-TOF-MS, Kore Technology). In the ATMECH project, the CIR-TOF-MS

103   was replaced with proton transfer reaction mass spectrometry (PTR-MS, Ionikon Analytik).

104   SOA mass, size and number concentrations were measured using a scanning mobility particle

105   sizer (TSI Incorporated, model 3080) consisting of a differential mobility analyzer (model

106   3081) and a condensation particle counter (model 3775).

107

108   **Aerosol Sampling and Analysis**

109   The analytical procedures are discussed in more detail in Pereira et al. (2014)[56] with a brief

110   summary given here. Aerosol samples were collected every 30 minutes using a PILS

111   (Brechtel Manufacturing, model 4002). The PILS inlet was connected to the chamber outlet

112   using 1.5 metres of 1/3" stainless steel tubing. PM_1 aerosol samples were collected using an

113   impactor at an average flow rate of 12 L min^{-1}. The PILS sample and wash flow was set to

114   200 µL min^{-1} and 240 µL min^{-1}, respectively, and consisted of optima LC-MS grade water

115   (Fisher Scientific, UK). After sample collection, PILS vials were securely sealed, wrapped in

116   foil to minimise potential degradation from photolysis and stored at − 20 °C until analysis.

117   Prior to analysis, PILS samples were evaporated to dryness using a V10 vacuum solvent

118   evaporator (Biotage, USA) and re-suspended in 50:50 methanol:water (optima LC-MS grade,

119   Fisher Scientific, UK).

120

121   SOA composition was investigated using an Agilent 1100 series HPLC (Berkshire, UK)

122   coupled to a HTC Plus ion trap mass spectrometer (IT-MS, Bruker Daltonics, Bremen,

123   Germany). A reversed phase Pinnacle C_{18} 150 mm x 4.6 mm, 5 µm particle size column

124   (Thames Resteck, UK) was used. The mobile phase consisted of water (optima LC-MS

6

125   grade) with 0.1 % formic acid (Sigma Aldrich, UK) and methanol (optima LC-MS grade,

126   Fisher Scientific UK). The MS was operated in alternating polarity mode, scanning from *m/z*

127   50 to 600. Tandem MS (collision induced dissociation, CID) was achieved through the

128   automated MS^2 function within the Esquire software (Bruker Daltonics, software version

129   5.2). In addition to the HPLC-ITMS, the ATMECH PILS samples were further investigated

130   using a solariX FTICR-MS with a 9.4-T superconducting magnet (Bruker Daltonics,

131   Coventry, UK) and a Dionex ultimate 3000 HPLC (Thermo Scientific Inc, UK) coupled to an

132   ultra high resolution QTOFMS (maXis 3G, Bruker Daltonics, Coventry, UK). The HPLC-

133   QTOFMS used the same reversed phase column and mobile phase composition as described

134   above for the HPLC-ITMS analysis. Spectral analysis was performed using DataAnalysis 4.0

135   software (Bruker Daltonics, Breman, Germany).

136

137   **Results and Discussion**

138   Initially, the PILS samples were screened for SOA species using HPLC-ITMS. Any

139   compounds present before the introduction of the VOC precursor and NO into the chamber

140   were excluded from further analysis. Only compounds that displayed changes in their

141   chromatographic peak areas were investigated further. Peak areas of the observed SOA

142   compounds were measured in each 30 minute PILS sample, allowing the temporal evolution

143   of individual species in the particulate phase to be observed. The temporal profiles of the

144   VOC precursor, NO, NO_2, O_3 and the SOA mass formed, during the experiments can be

145   found in the SI, Figure S1. The observed first generation gas-phase photo-oxidation products

146   are shown in the SI, Figure S2.

147

148   **Photo-oxidation of Methyl Chavicol**

7

149   Initially, the SOA composition formed during the photo-oxidation of methyl chavicol,

150   experiment MC$_{[high]}$ (Table 1) was investigated. In this experiment, 460 ppbv of methyl

151   chavicol and 92 ppbv of NO were added into the chamber and the chamber exposed to

152   sunlight. The maximum SOA mass formed was 283 µg m^{-3}, resulting in an SOA yield of 31

153   %[56] (corrected for chamber wall loss and dilution). In total, 79 SOA compounds were

154   observed in the PILS SOA samples using HPLC-ITMS; including 20 SOA compounds in

155   addition to those previously reported[56]. Temporal profiles were created for 70 of the 79 SOA

156   species. The other 9 compounds were excluded owing to the majority of chromatographic

157   peaks observed being below the limit of detection (defined as S/N = 3). The temporal profiles

158   of the individual SOA species varied considerably, with different rates of aerosol partitioning,

159   formation and loss observed. Nevertheless, three main temporal profile shapes could be

160   distinguished.

161

162   The majority of SOA compounds displayed a relatively slow increase in their particle phase

163   concentration, following initial aerosol growth, after which their concentration either

164   plateaued or began to decrease towards the end of the experiment (~ 4 hours). Of the 79 SOA

165   compounds observed, 47 species displayed this type of temporal profile (hereafter referred to

166   as TP1) and an example is shown in Figure 1A. The majority of these compounds were first

167   observed in the aerosol phase between 71 to 101 minutes into the experiment, when the SOA

168   mass in the chamber was rapidly increasing (63 to 188 µg m^{-3}, Figure 1G). All of these

169   compounds displayed a gradual increase in their particulate phase concentration, with the

170   majority reaching maximum concentration at ~ 175 minutes into the experiment, when SOA

171   formation in the chamber had plateaued. The compound structures of 5 of these species have

172   been determined[56] and were identified as; (3-hydroxy-4-methoxyphenyl)acetic acid, 3-(3-

173   hydroxy-4-methoxyphenyl)propane-1,2-diol,   4-methoxybenzoic   acid,   3-hydroxy-4-

8

174   methoxybenzoic   acid   and   2-hydroxy-3-(3-hydroxy-4-methoxyphenyl)propanal.   The

175   saturation concentrations (C^* (μg m^{-3}))[57] of these compounds were calculated (see SI) and

176   determined to range from 1.23 to 917 μg m^{-3}, characterising these species as intermediate- to

177   semi-VOCs (IVOC-SVOC). The compound structures, their most likely mechanistic

178   generation and the time period these compounds were first observed in the aerosol phase are

179   shown in SI, Table S1.

180

181   The mass fraction (y_i) of a species in the aerosol phase can be calculated by dividing the

182   measured concentration of species (i) in the condensed phase ($C_{i,aer}$ (μg m^{-3})) by the average

183   SOA mass formed (C_{OA} (μg m^{-3})) in each PILS sampling time period ($y_i = C_{i,aer}/C_{OA}$)[58]. The

184   measured mass fraction (y_i) of 4-methoxybenzoic acid (typical TP1 species) in the condensed

185   phase displayed a linear increase (R^2 = 0.9938) with time, after ~101 minutes into the

186   experiment (SOA mass > 191 μg m^{-3}), as shown in Figure 1B. The gas-phase concentration

187   of 4-methoxybenzoic acid could not be determined due to the extensive fragmentation of this

188   species in the PTR-MS. However based on the absorptive partitioning theory[58], a positive

189   linear relationship between y_i and time would only be observed if the gas-phase concentration

190   ($C_{i,gas}$ (μg m^{-3})) of this species continued to increase linearly throughout the experiment;

191   where $C_{i,gas} = (C_i^* \times C_{i,aer})/C_{OA}$[58]. It is therefore suggested that the positive linear relationship

192   observed here, is a result of a faster gas-phase formation rate than loss, resulting in

193   progressive absorptive partitioning into the aerosol phase as $C_{i,gas}$ and C_{OA} increases[4, 59, 60].

194   The majority of the TP1 compounds displayed a linear relationship with the SOA mass,

195   suggesting the partitioning of these species into the aerosol phase were also driven by

196   absorptive partitioning, which considering the relatively high volatility of the identified

197   species, would appear to be a reasonable explanation. There were however, variations in the

198   timing, duration and rate of increasing/decreasing y_i, most likely owing to the different rates

9

199   of formation and loss of these compounds in the gas-phase and their volatility. Reactive

200   uptake *via* in-particle formation processes[58] is also a possibility, however it is unclear if the

201   formation of the TP1 species (*i.e.* 59 % of observed compounds) through in-particle phase

202   reactions would result in a linear relationship with the SOA mass.

203

204   The second type of temporal profile shape observed (TP2) displayed a rapid increase and

205   then decrease in aerosol phase concentration, as shown in Figure 1C. These species were

206   short lived, remaining in the aerosol phase for a maximum of 2.5 hours, and could not be

207   detected in the aerosol samples taken at the end of the experiment. Only 3 compounds

208   displayed this type of temporal profile and the structure of one was identified as (4-

209   methoxyphenyl)acetic acid[56]. The two unidentified species consisted of one highly

210   oxygenated compound, $C_8H_{12}O_8$ (O:C = 1) and one species, $C_{11}H_{14}O_4$, which contained one

211   more carbon atom than the original VOC precursor. All of these compounds reached peak

212   concentration up to 30 minutes after partitioning into the aerosol phase (*i.e.* in the following

213   PILS sample) and displayed a rapid loss process after maximum concentration was observed.

214   The rapid decrease in the aerosol phase concentration observed for these compounds could be

215   due to a variety of loss processes, such as; (i) photolysis or further reaction of the compound

216   in the gas-phase resulting in re-volatilisation from the particle phase; and/or, (ii) in-particle

217   phase/heterogeneous reactions.

218

219   For the identified species, (4-methoxyphenyl)acetic acid, photolytic degradation is

220   considered to be negligible[61]. However, the identification of an oxidation product, with an

221   additional ˙OH group on the aromatic ring (3-hydroxy-4-methoxyphenyl)acetic acid[56]

222   indicates further that gas-phase and/or heterogeneous reactions are occurring. The measured

223   mass fraction (y_i) of (4-methoxyphenyl)acetic acid in the condensed phase decreased linearly

10

224　　with time (R^2 = 0.9903, Figure 1D). Assuming equilibrium partitioning, the temporal

225　　evolution of (4-methoxyphenyl)acetic acid in the aerosol phase can be predicted by using

226　　C_{iaer} = ($C_{OA} \times C_{igas}$)/C^{*58}. The predicted and measured particulate phase temporal profiles of

227　　(4-methoxyphenyl)acetic acid are shown in the SI, Figure S3. There are clear differences

228　　between the two profiles, with the predicted temporal profile timing and shape more closely

229　　resembling TP1 than a TP2 evolution. This suggests that for these species an additional loss

230　　process is occurring, such as in-particle phase/heterogeneous reactions, leading to a deviation

231　　from gas-particle equilibrium partitioning.

232

233　　　The third type of temporal profile shape (TP3) was similar to TP2 discussed above, except

234　　these compounds appeared in the aerosol phase earlier in the experiment (between 41 to 71

235　　minutes) and a different rate of decreasing aerosol concentration was observed (Figure 1E).

236　　Interestingly, all 8 species that displayed this type of temporal profile contained nitrogen.

237　　Seven of these organic nitrogen (ON) species were first observed in the aerosol phase when

238　　initial SOA growth was observed in the chamber (41 - 71 minutes into the experiment, Figure

239　　1E) and reached peak concentration within the next 30 minutes. The complex re-

240　　arrangements observed for these compounds during CID in the mass spectrometer made the

241　　structural identification particularly difficult. However, one of these compounds was

242　　identified as 3-(5-hydroxy-4-methoxy-2-nitrophenyl)propane-1,2-diol[56] and the structures of

243　　two others have been tentatively assigned as substituted nitrophenols; 5-methoxy-4-nitro-2-

244　　(prop-2-en-1-yl)phenol and 1-hydroxy-3-(2-hydroxy-4-methoxy-5-nitrophenyl)propan-2-one

245　　(see the SI for the discussion of the structural assignment). The compound structures, time

246　　period these compounds were first observed in the aerosol phase and their proposed

247　　mechanistic generations are shown in SI Table S2. The calculated saturation concentrations

248　　and O:C ratios of the structurally identified compounds ranged from 4.37×10^2 to 2.86×10^{-3}

11

249 μg m^{-3} and 0.4 to 0.6 respectively, classifying these species as semi- to low volatility organic

250 compounds (SVOC-LVOC)[39].

251

252   The decrease in the particulate phase concentration observed for these species may be the

253 result of a number of competing processes, such as; the low formation rates of the gas-phase

254 nitro-aromatics as the NO_2 concentration is depleted in the chamber (as NO_x is not

255 replenished), photolysis/further reaction of the gas-phase species which may lead to re-

256 volatilisation from the aerosol phase and/or in-particle phase/heterogeneous chemistry.

257 However, the observation of only one additional nitrogen containing compound later in the

258 experiment suggests that either; (i) these compounds are entirely removed from the aerosol

259 phase through re-volatilisation and do not partition back into the aerosol phase, or; (ii) upon

260 further reaction lose nitrogen. The complete removal of these species from the particulate

261 phase through re-volatilisation would appear unlikely due to the low volatility of these

262 compounds. A more likely explanation for the lack of additional nitrogen containing

263 oxidation products, is that upon further reaction, nitrogen is being lost. A number of recent

264 studies have found that nitrophenols can lose HONO in the gas phase[62-64]; potentially a

265 similar loss mechanism could also occur in the condensed phase, explaining why only one

266 additional nitrogen containing oxidation product was observed. In contrast to the temporal

267 profiles discussed above, the measured mass fraction (y_i) of all of the TP3 compounds

268 displayed a decreasing exponential relationship with time ($R^2 > 0.9432$). This relationship

269 can be observed in Figure 1F for the identified species, 3-(5-hydroxy-4-methoxy-2-

270 nitrophenyl)propane-1,2-diol. The reason why an exponential relationship is observed is

271 currently unclear but possible influences are discussed further below.

272

273 **Evolution of Nitrophenols**

12

274   SOA was first observed in the PILS sample collected between 41 to 71 minutes into the

275   experiment (SI Figure S4). In this sample, 13 SOA compounds were observed and included

276   eight ON species ($C_9H_{11}NO_9$ (t_R = 11.8), $C_9H_{11}NO_9$ (t_R = 12.8), $C_{10}H_9NO_3$, $C_{10}H_{13}NO_6$,

277       $C_{10}H_{11}NO_6$, $C_{10}H_{11}NO_4$, $C_5H_7NO_6$ and $C_{10}H_{17}NO_3$), one oligomer ($C_{18}H_{20}O_{12}$), three oxidised

278   compounds ($C_{10}H_{14}O_3$, $C_{11}H_{18}O_5$ and $C_{10}H_{12}O_5$), and one compound at molecular weight

279   (MW) 120 g mol^{-1}; whose molecular formula could not be assigned using only the elements

280   C, H, N and O. Of the ON compounds, the structures of three were identified as substituted

281   nitrophenols (3-(5-hydroxy-4-methoxy-2-nitrophenyl)propane-1,2-diol[56], (SI Table S2,

282   compound 1), 1-hydroxy-3-(2-hydroxy-4-methoxy-5-nitrophenyl)propan-2-one (SI Table S2,

283   compound 2) and 5-methoxy-4-nitro-2-(prop-2-en-1-yl)phenol (SI Table S2, compound 3),

284   see SI for the structural assignment) and a further three displayed characteristic fragmentation

285   patterns suggesting these compounds contained a resonance stabilised ring structure and a

286   nitro group ($C_9H_{11}NO_9$ (t_R = 11.8), $C_9H_{11}NO_9$ (t_R = 12.8) and $C_{10}H_9NO_3$), indicating that

287   these species were also likely to be substituted nitrophenols.

288

289   The particulate phase temporal profiles of the nitrophenols (both identified and suspected)

290   and the NO_2/NO (ppbv/ppbv) ratio were found to be remarkably similar, as shown for

291   example in Figure 2. All of the structurally identified nitrophenols were observed to have

292   different degrees of oxidation on the hydrocarbon chain substituent, with a diol, hydroxy-

293   carbonyl and unreacted alkene (same functionality as the starting precursor, methyl chavicol)

294   observed. Nevertheless, all of these compounds displayed the same temporal profile shape

295   and relationship with the NO_2/NO ratio, suggesting that it is the NO_2 group on the aromatic

296   ring that controls the partitioning, formation and loss of these species in the particulate phase.

297   This can be further supported by considering the two remaining ON compounds observed,

298       $C_5H_7NO_6$ and $C_{10}H_{17}NO_3$. Both of these compounds displayed a TP1 temporal profile shape

13

299   rather than the nitrophenol TP3 shape. Based on the molecular formulae, these species cannot

300   contain a resonance stabilised ring structure (*i.e.* they are ring opened species) with $C_5H_7NO_6$

301   containing too few carbon atoms, and $C_{10}H_{17}NO_3$ containing too many hydrogen atoms.

302   Thus, these compounds cannot be substituted nitrophenols, potentially explaining why a TP3

303   evolution and relationship with the NO_2/NO ratio was not observed for these species.

304

305   The structurally identified nitrophenols were characterised as SVOCs to LVOCs, with 3-(5-

306   hydroxy-4-methoxy-2-nitrophenyl)propane-1,2-diol just fractionally outside the nucleator

307   (ELVOC) region proposed in Donahue et al. (2013)[26]. Converting the calculated saturation

308   concentrations of 3-(5-hydroxy-4-methoxy-2-nitrophenyl)propane-1,2-diol ($C^* = 2.86 \times 10^{-3}$

309    $\mu g\ m^{-3}$) and 1-hydroxy-3-(2-hydroxy-4-methoxy-5-nitrophenyl)propan-2-one ($1.09 \times 10^{-1}\ \mu g$

310   m^{-3}) into gas-phase mixing ratios, concentrations of 0.29 pptv and 11.05 pptv, respectively,

311   would be required for these compounds to reach their saturation concentrations and partition

312   into the aerosol phase without any absorptive mass present. Considering the initial mixing

313   ratio of methyl chavicol (460 ppbv), the saturation concentrations of these suspected third

314   generation products would appear to be easily obtainable. Furthermore, the molecular

315   formulae of two of the suspected nitrophenols were found to have one less carbon atom than

316   these species, but considerably more oxygen atoms (O_9 instead of O_6 ($C_9H_{11}NO_9$, O:C =1))

317   indicating these compounds are also likely to be of similar or lower volatility. The low

318   saturation concentrations of these compounds coupled with the observation of these species

319   in the aerosol phase during initial SOA growth, as shown in Figure 3, suggests these species

320   could potentially be involved new particle formation and/or SOA growth.

321

322   **Toluene and 4-Methyl Catechol: Nitrophenol Evolution**

14

323　　　Owing to the clear importance of nitrophenols in methyl chavicol SOA formation, two

324　　other aromatic systems, toluene and 4-methylcatechol were also investigated. Two toluene

325　　photo-oxidation experiments were investigated; (i) Tol_{low}, a VOC/NO_x ratio of ~ 13, where

326　　535 ppbv of toluene and 41 ppbv of NO was added into the chamber, and; (ii) Tol_{mod}, a

327　　higher VOC/NO_x ratio of ~ 5, where 560 ppbv of toluene and 105 ppbv of NO was added

328　　into the chamber (Table 1). The maximum amount of SOA mass formed was 22.3 μg m^{-3} in

329　　Tol_{low} and 32.8 μg m^{-3} in Tol_{mod}, with SOA yields of 3.4 % and 5.4 % respectively (corrected

330　　for wall loss and chamber dilution). In both experiments, two nitrogen containing compounds

331　　were observed in the PILS SOA samples and are assigned as 2-methyl-4-nitrophenol

332　　($C_7H_7NO_3$, MW 153 g mol^{-1}), a second generation product, and methyl nitro-catechol

333　　($C_7H_7NO_4$, MW 169 g mol^{-1}), a third generation product. Both of these compounds are

334　　known toluene photo-oxidation products[65-69]. The identification of 2-methyl-4-nitrophenol

335　　was confirmed from the chromatographic retention time and fragmentation patterns of the

336　　commercially available standard. The exact locations of the aromatic substitutions of methyl

337　　nitro-catechol are unclear and are discussed in the SI, but based on known gas-phase

338　　mechanisms and the structural elucidation of the mass spectral fragmentation patterns, the

339　　most likely structure is 3-methyl-4-nitrocatechol.

340

341　　　The temporal profiles of 2-methyl-4-nitrophenol and methyl nitro-catechol were observed

342　　to follow the same TP3 shape observed previously for the methyl chavicol nitrophenols.

343　　Again, both of these compounds displayed a relationship with the temporal profile of the

344　　NO_2/NO ratio (SI Figure S5 and S6). The saturation concentrations of 2-methyl-4-nitrophenol

345　　and methyl nitro-catechol (calculation based on 3-methyl-4-nitrocatechol) were determined

346　　as 1.12×10^5 and 1.41×10^3 μg m^{-3}, respectively, characterising these species as IVOCs. The

347　　gas-phase concentrations of 2-methyl-4-nitrophenol and methyl nitro-catechol in both toluene

15

348   experiments are not known. However, in order for 2-methyl-4-nitrophenol and methyl nitro-

349   catechol to partition into the aerosol phase without any absorptive mass present, gas-phase

350   concentrations of 17.95 ppmv and 0.20 ppmv, respectively, would be required (based on their

351   calculated saturation concentrations); well in excess of the amount of toluene reacted prior to

352   SOA formation in both experiments. Providing some absorptive mass is present, a gaseous

353   species can partition some of its mass into the aerosol phase below its saturation

354   concentration[4, 59, 60]. However, taking this into account, equilibrium partitioning cannot

355   describe the observation of these relatively volatile species in the aerosol phase during initial

356   aerosol formation and growth (see SI for the supporting calculations and SI Figures S7 and

357   S8).

358

359   The reason why these IVOCs are observed in the aerosol phase during initial aerosol

360   growth is currently unclear. However, a recent study has also observed a similar phenomenon

361   with nitrophenols formed from the photo-oxidation of benzene[70]. Using high resolution time-

362   of-flight aerosol mass spectrometry (HR-TOF-AMS), Sato et al. (2012) measured

363   nitrophenols from the onset of SOA nucleation and observed them to rapidly decrease in

364   concentration over the first hour[70]. The composition of these compounds was determined

365   from the collection of SOA onto filter samples, followed by offline HPLC-TOFMS

366   analysis[70]. Whilst no reference to volatility was made in their study, the two nitrophenols

367   identified (4-nitrophenol and 4-nitrocatechol) are of even higher volatility (calculated C^* =

368   3.19 x 10^5 and 4.70 x 10^3 µg m^{-3}) than the species identified in this study, owing to the lack of

369   a methyl group on the aromatic ring. Furthermore, Sato et al. (2012) observed that from the

370   onset of SOA nucleation to the first 60 minutes of their experiment, nitrophenol formation

371   was almost independent of the amount of absorptive mass present[70], which is in agreement

16

372   with the results shown here. One possible explanation for these observations is the formation

373   of gas-phase clusters.

374

375   A number of studies have shown phenol-phenol or phenol-water clusters can form in the

376   gas-phase and produce stable clusters through hydrogen bonding[71-74]. Theoretical simulations

377   predict the stability of phenol-water clusters to be comparable to that of water clusters,

378   exhibiting similar hydrogen bonding energies[72, 74]. Whilst no studies have investigated

379   nitrophenol gas-phase clustering, these compounds are known to form both intra- and inter-

380   molecular hydrogen bonds; with very strong intra-molecular hydrogen bonding observed

381   between the nitro and hydroxyl group (C-NO—HO-C)[75-77]. Such interactions could result in

382   stabilised cluster formation and new particle formation, potentially accounting for the

383   observations shown in Sato et al. (2012)[70] and in this study; although this remains to be

384   explained.

385

386   In contrast to the other two aromatic systems investigated, the photo-oxidation of 4-

387   methylcatechol (Table 1) did not result in the formation of nitrophenols in the aerosol phase

388   during initial SOA growth. In this experiment, 591 ppbv of 4-methyl catechol and 120 ppbv

389   of NO were added into the chamber, resulting in the formation of 154 $\mu g\ m^{-3}$ of SOA mass,

390   with an SOA yield of 9.8 % (corrected for wall loss and chamber dilution). Only one

391   nitrophenol compound (MW 168 g mol^{-1}, 4-methyl-5-nitrocatechol) was observed in the

392   PILS SOA samples. The fragmentation patterns and structural assignment of this species is

393   discussed in the SI, but based on known gas-phase mechanisms and the characteristic mass

394   spectral fragmentation patterns, the most likely structure is 4-methyl-5-nitrocatechol.

395   Interestingly, 4-methyl-5-nitrocatechol was not observed in the aerosol phase until the

396   chamber covers were closed, approximately 2.5 hours after irradiation was initiated (SI

17

397   Figure S9). The observation of this species in the aerosol phase after irradiation had stopped,

398   suggests photolytic dissociation is preventing this compound from accumulating in the gas-

399   phase and partitioning into the aerosol phase. This also indicates that there is a dark formation

400   source of 4-methyl-5-nitrocatechol which is most likely initiated through the rapid reaction of

401   4-methylcatechol with NO_3 ($13.4 \pm 5.0 \times 10^{-11}$ cm^3 $molecule^{-1}$ s^{-1})[78] followed by the addition

402   of NO_2 to the aromatic ring.

403

404   The location of aromatic substitutions can affect the rate of reaction[79], photolytic

405   dissociation[79, 80] (including HONO formation[63]) and the strength of hydrogen bonds owing to

406   the change in resonance stability of the aromatic ring (should these species undergo gas-

407   phase clustering)[75-77]. It is therefore likely that the location of aromatic substitutions in 4-

408   methyl-5-nitrocatechol makes this compound more susceptible to a loss process such as

409   photolysis than 3-methyl-4-nitrocatechol (observed from the photo-oxidation of toluene),

410   accounting for the differences in the timing of partitioning observed; highlighting the

411   importance of studying SOA formation at molecular level.

412

413   **Atmospheric Relevance**

414   In chamber experiments, the $RO_2 + RO_2$ reaction pathway favoured in relatively "low NO

415   environments" is thought to be key to new particle formation and SOA growth in the photo-

416   oxidation of aromatic VOC systems[48]. Here we observed that both a low NO environment

417   and sufficient NO_2 concentration is required for the formation of ON compounds, which in

418   the photo-oxidation of methyl chavicol represented 8 of the 13 particulate phase compounds

419   observed during initial aerosol growth. The ON compounds at their maximum concentration

420   represented 4.39 % of SOA mass in $MC_{[high]}$, 1.05 % in Tol_{mod} and 0.18 % in Tol_{low}, based on

421   the average SOA mass formed during the same PILS sampling time period. In chamber

18

422   experiments, where NO_x is not replenished, the NO_2 concentration decreases below the

423   detection limit of the instrument ($\sim$ 0.6 ppbv), which is likely to reduce the formation rate of

424   the ON species. However, in the atmosphere NO_2 continuously forms within the VOC-NO_x-

425   O_3 cycle, which is likely to result in the continuous formation of these compounds in the

426   ambient atmosphere. For the toluene (no kinetic data exists for methyl chavicol) in polluted

427   environments, hydrogen atom abstraction and addition of NO_2 to the aromatic ring (2.5-3.6 $\times$

428   10^{-11} cm^3 molecule^{-1} s^{-1})[81] is a minor, but still important, channel in competition with the

429   addition of O_2 (1.8-20 $\times$ 10^{-16} cm^3 molecule^{-1} s^{-1})[82]. Close to emission sources, NO_2 will be

430   rapidly formed *via* the conversion of NO, leading to relatively high NO_2 concentrations,

431   increasing the potential to form these species[81, 82]. Peroxyacetyl nitrates (PANs) may also

432   contribute to the formation of these ON species, providing a source of NO_2 upon thermal

433   decomposition[83]. Recent literature has suggested that only pptv concentrations of ELVOCs

434   would be required to drive new particle formation and subsequent growth[26].

435

436   The chemistry simulated in these experiments will be representative of VOC emissions

437   near a pollution source (*i.e.* high NO concentrations) and their chemical transformations as

438   they travel downwind into cleaner environments (*i.e.* conversion of NO to NO_2, followed by

439   the photolysis of NO_2 to form O_3). The initial VOC:NO_x ratio in experiment MC[high] is

440   representative of an agro-industrialised oil palm plantation in northern Borneo (see Pereira et

441   al. (2014)[56] for further information). In the case of the toluene photo-oxidation experiments,

442   the respectively defined "low" and "moderate" NO_x experiments (VOC:NO_x 5:1 and 13:1;

443   Table 1) were performed under NO_x-limited ozone formation conditions (as often

444   experienced in southern Europe[45] and suburban China[84]). The initial VOC:NO_x ratios in both

445   the toluene and catechol (VOC:NOx = 5:1) experiments were selected using detailed

446   chemical chamber simulations to construct ozone isopleth plots (see Bloss et al. (2005)[45] for

447   further information) to give maximum ozone formation[85].

448

449   The involvement of the ON species in new particle formation and SOA growth was not

450   directly measured. However, the observation of various nitrophenols of differing volatilities

451   in the condensed phase during initial aerosol growth in the photo-oxidation of methyl

452   chavicol and toluene, suggests these compounds may be participating new particle formation

453   and/or SOA growth. Further study, such as measurements with an atmospheric pressure

454   ionisation mass spectrometer and quantum calculations of binding energies, is warranted to

455   investigate this. Using the techniques described, a greater insight and knowledge of the

456   dynamic processes affecting SOA formation and evolution on a molecular level can be

457   obtained. To our knowledge, this is the first experimental evidence of variable temporal

458   profiles of speciated SOA compounds as a function of photochemical ageing. As shown in

459   this work, the partitioning, formation and loss of individual compounds in the particle phase

460   can vary considerably with only slight changes in the chemical composition and structure.

461   Understanding why different compounds display different rates of formation and loss is

462   critical to understanding SOA formation and evolution in the ambient atmosphere.

463

464   **Acknowledgements**

20

477

Supporting Information

479   SI Tables S1 and S2 show the proposed mechanistic generations of the structurally identified

480   compounds displaying TP1 or TP3 evolutions. Figure S1 displays the temporal profiles of the

481   VOC precursors, NO, NO_2, O_3 and SOA mass formed, and Figure S2 displays the observed

482   first generation gas-phase oxidation products formed in the experiments discussed. Figure S3

483   displays the predicted and measured condensed phase temporal profile of (4-

484   methoxyphenyl)acetic acid. Figures S4 to S9 display the relationship of ON temporal profiles

485   with the NO_2/NO ratio in Tol_{mod} and Tol_{low} and contour plots of particle diameter *vs.* particle

486   mass and particle number for experiments Tol_{mod}, Tol_{low} and 4MCat. Tables S3 to S6 and

487   Figures S10 to S13, show the mass spectral fragment ions, proposed fragmentation and the

488   suggested ON compound structures. Finally, the PILS collection efficiency, volatility

489   calculations, particle wall loss corrections, quantification of the observed compounds and the

490   supporting calculations for the predicted 2-methyl-4-nitrophenol aerosol phase concentrations

491   are discussed. This information is available free of charge via the Internet at

492   http://pubs.acs.org/.

21

References

493   1.   Kanakidou, M.; Seinfeld, J. H.; Pandis, S. N.; Barnes, I.; Dentener, F. J.; Facchini, M.

494   C.; Van Dingenen, R.; Ervens, B.; Nenes, A.; Nielsen, C. J.; Swietlicki, E.; Putaud, J. P.;

495   Balkanski, Y.; Fuzzi, S.; Horth, J.; Moortgat, G. K.; Winterhalter, R.; Myhre, C. E. L.;

496   Tsigaridis, K.; Vignati, E.; Stephanou, E. G.; Wilson, J., Organic aerosol and global climate

497   modelling: A review. *Atmos. Chem. Phys.* **2005,** *5*, (4), 1053.

498   2.   Zhao, Y.; Kreisberg, N. M.; Worton, D. R.; Isaacman, G.; Weber, R. J.; Liu, S.; Day,

499   D. A.; Russell, L. M.; Markovic, M. Z.; VandenBoer, T. C.; Murphy, J. G.; Hering, S. V.;

500   Goldstein, A. H., Insights into secondary organic aerosol formation mechanisms from

501   measured gas/particle partitioning of specific organic tracer compounds. *Environ. Sci.*

502   *Technol.* **2013,** *47*, (8), 3781.

503   3.   Williams, B.; Goldstein, A.; Kreisberg, N.; Hering, S.; Worsnop, D.; Ulbrich, I.;

504   Docherty, K.; Jimenez, J., Major components of atmospheric organic aerosol in southern

505   california as determined by hourly measurements of source marker compounds. **2010,** *10*,

506   (23), 11577.

507   4.   Kroll, J. H.; Seinfeld, J. H., Chemistry of secondary organic aerosol: Formation and

508   evolution of low-volatility organics in the atmosphere. *Atmos. Environ.* **2008,** *42*, (16), 3593.

509   5.   Hallquist, M.; Wenger, J. C.; Baltensperger, U.; Rudich, Y.; Simpson, D.; Claeys, M.;

510   Dommen, J.; Donahue, N. M.; George, C.; Goldstein, A. H.; Hamilton, J. F.; Herrmann, H.;

511   Hoffmann, T.; Iinuma, Y.; Jang, M.; Jenkin, M. E.; Jimenez, J. L.; Kiendler-Scharr, A.;

512   Maenhaut, W.; McFiggans, G.; Mentel, T. F.; Monod, A.; Prévôt, A. S. H.; Seinfeld, J. H.;

513   Surratt, J. D.; Szmigielski, R.; J., W., The formation, properties and impact of secondary

514   organic aerosol: Current and emerging issues. *Atmos. Chem. Phys.* **2009,** *9*, (14), 5155.

515   6.   Hearn, J. D.; Renbaum, L. H.; Wang, X.; Smith, G. D., Kinetics and products from

516   reaction of cl radicals with dioctyl sebacate (dos) particles in o2: A model for radical-initiated

517   oxidation of organic aerosols. *PCCP* **2007,** *9*, (34), 4803.

518   7.   Claeys, M.; Wang, W.; Ion, A. C.; Kourtchev, I.; Gelencsér, A.; Maenhaut, W.,

519   Formation of secondary organic aerosols from isoprene and its gas-phase oxidation products

520   through reaction with hydrogen peroxide. *Atmos. Environ.* **2004,** *38*, (25), 4093.

521   8.   Perri, M. J.; Seitzinger, S.; Turpin, B. J., Secondary organic aerosol production from

522   aqueous photooxidation of glycolaldehyde: Laboratory experiments. *Atmos. Environ.* **2009,**

523   *43*, (8), 1487.

524   9.   George, I.; Abbatt, J., Chemical evolution of secondary organic aerosol from oh-

525   initiated heterogeneous oxidation. *Atmos. Chem. Phys*. **2010,** *10*, (12), 5551.

526   10.   Barsanti, K. C.; Pankow, J. F., Thermodynamics of the formation of atmospheric

527   organic particulate matter by accretion reactions - part 1: Aldehydes and ketones. *Atmos.*

528   *Environ.* **2004,** *38*, (26), 4371.

529   11.   Kalberer, M.; Paulsen, D.; Sax, M.; Steinbacher, M.; Dommen, J.; Prevot, A.; Fisseha,

530   R.; Weingartner, E.; Frankevich, V.; Zenobi, R., Identification of polymers as major

531   components of atmospheric organic aerosols. *Science* **2004,** *303*, (5664), 1659.

532   12.   Tolocka, M. P.; Jang, M.; Ginter, J. M.; Cox, F. J.; Kamens, R. M.; Johnston, M. V.,

533   Formation of oligomers in secondary organic aerosol. *Environ. Sci. Technol.* **2004,** *38*, (5),

534   1428.

535   13.   Iinuma, Y.; Böge, O.; Gnauk, T.; Herrmann, H., Aerosol-chamber study of the α -

536   pinene/o3 reaction: Influence of particle acidity on aerosol yields and products. *Atmos.*

537   *Environ.* **2004,** *38*, (5), 761.

23

538   14.   Gao, S.; Keywood, M.; Ng, N. L.; Surratt, J.; Varutbangkul, V.; Bahreini, R.; Flagan,

539   R. C.; Seinfeld, J. H., Low-molecular-weight and oligomeric components in secondary

540   organic aerosol from the ozonolysis of cycloalkenes and α-pinene. *J. Phys. Chem. A* **2004,**

541   *108*, (46), 10147.

542   15.   Gao, S.; Ng, N. L.; Keywood, M.; Varutbangkul, V.; Bahreini, R.; Nenes, A.; He, J.;

543   Yoo, K. Y.; Beauchamp, J. L.; Hodyss, R. P.; Flagan, R. C.; Seinfeld, J. H., Particle phase

544   acidity and oligomer formation in secondary organic aerosol. *Environ. Sci. Technol.* **2004,** *38*,

545   (24), 6582.

546   16.   Goldstein, A. H.; Galbally, I. E., Known and unexplored organic constituents in the

547   earth's atmosphere. *Environ. Sci. Technol.* **2007,** *41*, (5), 1514.

548   17.   Zhang, R.; Suh, I.; Zhao, J.; Zhang, D.; Fortner, E. C.; Tie, X.; Molina, L. T.; Molina,

549   M. J., Atmospheric new particle formation enhanced by organic acids. *Science* **2004,** *304*,

550   (5676), 1487.

551   18.   Donahue, N. M.; Ortega, I. K.; Chuang, W.; Riipinen, I.; Riccobono, F.;

552   Schobesberger, S.; Dommen, J.; Baltensperger, U.; Kulmala, M.; Worsnop, D. R.;

553   Vehkamaki, H., How do organic vapors contribute to new-particle formation? *Faraday*

554   *discussions* **2013, 165, (0), 91**.

555   19.   Kulmala, M.; Kontkanen, J.; Junninen, H.; Lehtipalo, K.; Manninen, H. E.; Nieminen,

556   T.; Petäjä, T.; Sipilä, M.; Schobesberger, S.; Rantala, P.; Franchin, A.; Jokinen, T.; Järvinen,

557   E.; Äijälä, M.; Kangasluoma, J.; Hakala, J.; Aalto, P. P.; Paasonen, P.; Mikkilä, J.; Vanhanen,

558   J.; Aalto, J.; Hakola, H.; Makkonen, U.; Ruuskanen, T.; Mauldin, R. L.; Duplissy, J.;

559   Vehkamäki, H.; Bäck, J.; Kortelainen, A.; Riipinen, I.; Kurtén, T.; Johnston, M. V.; Smith, J.

560   N.; Ehn, M.; Mentel, T. F.; Lehtinen, K. E. J.; Laaksonen, A.; Kerminen, V.-M.; Worsnop, D.

561   R., Direct observations of atmospheric aerosol nucleation. *Science* **2013,** *339*, (6122), 943.

24

562 20. Donahue, N. M.; Trump, E. R.; Pierce, J. R.; Riipinen, I., Theoretical constraints on

563 pure vapor-pressure driven condensation of organics to ultrafine particles. *Geophys. Res. Lett.*

564 **2011,** *38*, (16), L16801.

565 21. Riipinen, I.; Pierce, J. R.; Yli-Juuti, T.; Nieminen, T.; Häkkinen, S.; Ehn, M.;

566 Junninen, H.; Lehtipalo, K.; Petäjä, T.; Slowik, J.; Chang, R.; Shantz, N. C.; Abbatt, J.;

567 Leaitch, W. R.; Kerminen, V. M.; Worsnop, D. R.; Pandis, S. N.; Donahue, N. M.; Kulmala,

568 M., Organic condensation: A vital link connecting aerosol formation to cloud condensation

569 nuclei (ccn) concentrations. *Atmos. Chem. Phys.* **2011,** *11*, (8), 3865.

570 22. Pierce, J. R.; Riipinen, I.; Kulmala, M.; Ehn, M.; Petäjä, T.; Junninen, H.; Worsnop,

571 D. R.; Donahue, N. M., Quantification of the volatility of secondary organic compounds in

572 ultrafine particles during nucleation events. *Atmos. Chem. Phys*. **2011,** *11*, (17), 9019.

573 23. Ehn, M.; Thornton, J. A.; Kleist, E.; Sipila, M.; Junninen, H.; Pullinen, I.; Springer,

574 M.; Rubach, F.; Tillmann, R.; Lee, B.; Lopez-Hilfiker, F.; Andres, S.; Acir, I.-H.; Rissanen,

575 M.; Jokinen, T.; Schobesberger, S.; Kangasluoma, J.; Kontkanen, J.; Nieminen, T.; Kurten,

576 T.; Nielsen, L. B.; Jorgensen, S.; Kjaergaard, H. G.; Canagaratna, M.; Maso, M. D.; Berndt,

577 T.; Petaja, T.; Wahner, A.; Kerminen, V.-M.; Kulmala, M.; Worsnop, D. R.; Wildt, J.;

578 Mentel, T. F., A large source of low-volatility secondary organic aerosol. *Nature* **2014,** *506*,

579 (7489), 476.

580 24. Wang, L.; Khalizov, A. F.; Zheng, J.; Xu, W.; Ma, Y.; Lal, V.; Zhang, R.,

581 Atmospheric nanoparticles formed from heterogeneous reactions of organics. *Nature Geosci*

582 **2010,** *3*, (4), 238.

583 25. Kokkola, H.; Yli-Pirilä, P.; Vesterinen, M.; Korhonen, H.; Keskinen, H.;

584 Romakkaniemi, S.; Hao, L.; Kortelainen, A.; Joutsensaari, J.; Worsnop, D. R.; Virtanen, A.;

25

585 Lehtinen, K. E. J., The role of low volatile organics on secondary organic aerosol formation.

586 *Atmos. Chem. Phys.* **2014,** *14*, (3), 1689.

587 26. Donahue, N.; Ortega, I.; Chuang, W.; Riipinen, I.; Riccobono, F.; Schobesberger, S.;

588 Dommen, J.; Baltensperger, U.; Kulmala, M.; Worsnop, D.; Vehkamaki, H., How do organic

589 vapors contribute to new-particle formation? *Faraday Discuss.* **2013,** *165*, 91

590 27. DeCarlo, P. F.; Kimmel, J. R.; Trimborn, A.; Northway, M. J.; Jayne, J. T.; Aiken, A.

591 C.; Gonin, M.; Fuhrer, K.; Horvath, T.; Docherty, K. S., Field-deployable, high-resolution,

592 time-of-flight aerosol mass spectrometer. *Anal. Chem.* **2006,** *78*, (24), 8281.

593 28. Canagaratna, M. R.; Jayne, J. T.; Jimenez, J. L.; Allan, J. D.; Alfarra, M. R.; Zhang,

594 Q.; Onasch, T. B.; Drewnick, F.; Coe, H.; Middlebrook, A.; Delia, A.; Williams, L. R.;

595 Trimborn, A. M.; Northway, M. J.; DeCarlo, P. F.; Kolb, C. E.; Davidovits, P.; Worsnop, D.

596 R., Chemical and microphysical characterization of ambient aerosols with the aerodyne

597 aerosol mass spectrometer. *Mass Spectrom. Rev.* **2007,** *26*, (2), 185.

598 29. Jimenez, J. L.; Canagaratna, M. R.; Donahue, N. M.; Prevot, A. S. H.; Zhang, Q.;

599 Kroll, J. H.; DeCarlo, P. F.; Allan, J. D.; Coe, H.; Ng, N. L.; Aiken, A. C.; Docherty, K. S.;

600 Ulbrich, I. M.; Grieshop, A. P.; Robinson, A. L.; Duplissy, J.; Smith, J. D.; Wilson, K. R.;

601 Lanz, V. A.; Hueglin, C.; Sun, Y. L.; Tian, J.; Laaksonen, A.; Raatikainen, T.; Rautiainen, J.;

602 Vaattovaara, P.; Ehn, M.; Kulmala, M.; Tomlinson, J. M.; Collins, D. R.; Cubison, M. J.; E.;

603 Dunlea, J.; Huffman, J. A.; Onasch, T. B.; Alfarra, M. R.; Williams, P. I.; Bower, K.; Kondo,

604 Y.; Schneider, J.; Drewnick, F.; Borrmann, S.; Weimer, S.; Demerjian, K.; Salcedo, D.;

605 Cottrell, L.; Griffin, R.; Takami, A.; Miyoshi, T.; Hatakeyama, S.; Shimono, A.; Sun, J. Y.;

606 Zhang, Y. M.; Dzepina, K.; Kimmel, J. R.; Sueper, D.; Jayne, J. T.; Herndon, S. C.;

607 Trimborn, A. M.; Williams, L. R.; Wood, E. C.; Middlebrook, A. M.; Kolb, C. E.;

608   Baltensperger, U.; Worsnop, D. R., Evolution of organic aerosols in the atmosphere. *Science*

609   **2009,** *326*, (5959), 1525.

610   30.   Laskin, A.; Laskin, J.; Nizkorodov, S. A., Mass spectrometric approaches for

611   chemical characterisation of atmospheric aerosols: Critical review of the most recent

612   advances. *Environ. Chem.* **2012,** *9*, (3), 163.

613   31.   Zhang, Q.; Jimenez, J. L.; Canagaratna, M. R.; Allan, J. D.; Coe, H.; Ulbrich, I.;

614   Alfarra, M. R.; Takami, A.; Middlebrook, A. M.; Sun, Y. L.; Dzepina, K.; Dunlea, E.;

615   Docherty, K.; DeCarlo, P. F.; Salcedo, D.; Onasch, T.; Jayne, J. T.; Miyoshi, T.; Shimono,

616   A.; Hatakeyama, S.; Takegawa, N.; Kondo, Y.; Schneider, J.; Drewnick, F.; Borrmann, S.;

617   Weimer, S.; Demerjian, K.; Williams, P.; Bower, K.; Bahreini, R.; Cottrell, L.; Griffin, R. J.;

618   Rautiainen, J.; Sun, J. Y.; Zhang, Y. M.; Worsnop, D. R., Ubiquity and dominance of

619   oxygenated species in organic aerosols in anthropogenically-influenced northern hemisphere

620   midlatitudes. *Geophys. Res. Lett.* **2007,** *34*, (13), L13801.

621   32.   Li, K.; Wang, W.; Ge, M.; Li, J.; Wang, D., Optical properties of secondary organic

622   aerosols generated by photooxidation of aromatic hydrocarbons. *Sci. Rep.* **2014,** *4*, 4922 .

623   33.   Singh, H. B.; Salas, L. J.; Cantrell, B. K.; Redmond, R. M., Distribution of aromatic

624   hydrocarbons in the ambient air. *Atmos. Environ. (1967)* **1985,** *19*, (11), 1911.

625   34.   Na, K.; Moon, K.-C.; Kim, Y. P., Source contribution to aromatic voc concentration

626   and ozone formation potential in the atmosphere of seoul. *Atmos. Environ.* **2005,** *39*, (30),

627   5517.

628   35.   Suthawaree, J.; Tajima, Y.; Khunchornyakong, A.; Kato, S.; Sharp, A.; Kajii, Y.,

629   Identification of volatile organic compounds in suburban bangkok, thailand and their

630   potential for ozone formation. *Atmos. Res.* **2012,** *104*, 245.

27

631   36.   Zi-feng, L.; Ji-ming, H. A. O.; Jing-chun, D.; Jun-hua, L. I., Estimate of the formation

632   potential of secondary organic aerosol in beijing summertime. *Huan Jing Ke Xue* **2009,** *30,*

633   969.

634   37.   Liu, S.; Ahlm, L.; Day, D. A.; Russell, L. M.; Zhao, Y.; Gentner, D. R.; Weber, R. J.;

635   Goldstein, A. H.; Jaoui, M.; Offenberg, J. H., Secondary organic aerosol formation from

636   fossil fuel sources contribute majority of summertime organic mass at bakersfield. *J.*

637   *Geophys. Res. Atmos.* **2012,** 177, (D24).

638   38.   Lü, Z.; Hao, J.; Duan, J.; Li, J., Estimate of the formation potential of secondary

639   organic aerosol in beijing summertime. *Huan jing ke xue= Huanjing kexue/[bian ji,*

640   *Zhongguo ke xue yuan huan jing ke xue wei yuan hui" Huan jing ke xue" bian ji wei yuan*

641   *hui.]* **2009,** *30,* (4), 969.

642   39.   de Gouw, J. A.; Brock, C. A.; Atlas, E. L.; Bates, T. S.; Fehsenfeld, F. C.; Goldan, P.

643   D.; Holloway, J. S.; Kuster, W. C.; Lerner, B. M.; Matthew, B. M.; Middlebrook, A. M.;

644   Onasch, T. B.; Peltier, R. E.; Quinn, P. K.; Senff, C. J.; Stohl, A.; Sullivan, A. P.; Trainer,

645   M.; Warneke, C.; Weber, R. J.; Williams, E. J., Sources of particulate matter in the

646   northeastern united states in summer: 1. Direct emissions and secondary formation of organic

647   matter in urban plumes. *J. Geophys. Res. Atmos.* **2008,** 113, (D8).

648   40.   Odum, J. R.; Jungkamp, T. P. W.; Griffin, R. J.; Flagan, R. C.; Seinfeld, J. H., The

649   atmospheric aerosol-forming potential of whole gasoline vapor. *Science* **1997,** *276,* (5309),

650   96.

651   41.   Gentner, D. R.; Isaacman, G.; Worton, D. R.; Chan, A. W. H.; Dallmann, T. R.;

652   Davis, L.; Liu, S.; Day, D. A.; Russell, L. M.; Wilson, K. R.; Weber, R.; Guha, A.; Harley, R.

653   A.; Goldstein, A. H., Elucidating secondary organic aerosol from diesel and gasoline vehicles

28

654   through detailed characterization of organic carbon emissions. *Proceedings of the National*

655   *Academy of Sciences* **2012,** *109*, (45), 18318.

656   42.   Odum, J. R.; Jungkamp, T. P. W.; Griffin, R. J.; Forstner, H. J. L.; Flagan, R. C.;

657   Seinfeld, J. H., Aromatics, reformulated gasoline, and atmospheric organic aerosol formation.

658   *Environ. Sci. Technol.* **1997,** *31*, (7), 1890.

659   43.   Xiao, H.; Zhu, B., Modelling study of photochemical ozone creation potential of non-

660   methane hydrocarbon. *Water, Air, Soil Pollut.* **2003,** *145*, (1-4), 3.

661   44.   Derwent, R.; Jenkin, M.; Passant, N.; Pilling, M., Reactivity-based strategies for

662   photochemical ozone control in europe. *Environ. Sci. Policy* **2007,** *10*, (5), 445.

663   45.   Bloss, C.; Wagner, V.; Bonzanini, A.; Jenkin, M. E.; Wirtz, K.; Martin-Reviejo, M.;

664   Pilling, M. J., Evaluation of detailed aromatic mechanisms (mcmv3 and mcmv3.1) against

665   environmental chamber data. *Atmos. Chem. Phys.* **2005,** *5*, (3), 623.

666   46.   Hurley, M. D.; Sokolov, O.; Wallington, T. J.; Takekawa, H.; Karasawa, M.; Klotz,

667   B.; Barnes, I.; Becker, K. H., Organic aerosol formation during the atmospheric degradation

668   of toluene. *Environ. Sci. Technol.* **2001,** *35*, (7), 1358.

669   47.   Johnson, D.; Jenkin, M. E.; Wirtz, K.; Martin-Reviejo, M., Simulating the formation

670   of secondary organic aerosol from the photooxidation of toluene. *Environ. Chem.* **2004,** *1*,

671   (3), 150.

672   48.   Song, C.; Na, K.; Warren, B.; Malloy, Q.; Cocker, D. R., Secondary organic aerosol

673   formation from the photooxidation of p- and o-xylene. *Environ. Sci. Technol.* **2007,** *41*, (21),

674   7403.

675   49.   Ng, N.; Kroll, J.; Chan, A.; Chhabra, P.; Flagan, R.; Seinfeld, J., Secondary organic

676   aerosol formation from m-xylene, toluene, and benzene. *Atmos. Chem. Phys.* **2007,** *7*, (14),

677   3909.

678   50.   Becker, K., Euphore: Final report to the european commission. *Contract EV5V-CT92-*

679   *0059, Bergische Universität Wuppertal, Germany* **1996**.

680   51.   Klotz, B.; Sørensen, S.; Barnes, I.; Becker, K. H.; Etzkorn, T.; Volkamer, R.; Platt,

681   U.; Wirtz, K.; Martín-Reviejo, M., Atmospheric oxidation of toluene in a large-volume

682   outdoor photoreactor: In situ determination of ring-retaining product yields. *J. Phys. Chem.*

683   *A.* **1998,** *102*, (50), 10289.

684   52.   Volkamer, R.; Platt, U.; Wirtz, K.; Barnes, I.; Sidebottom, H. *The european*

685   *photoreactor (euphore), 3rd annual report 2000*; Bergische Universität Wuppertal

686   Wuppertal, Germany: 2001.

687   53.   Muñoz, A.; Vera, T.; Sidebottom, H.; Mellouki, A.; Borrás, E.; Ródenas, M.;

688   Clemente, E.; Vázquez, M., Studies on the atmospheric degradation of chlorpyrifos-methyl.

689   *Environ. Sci. Technol.* **2011,** *45*, (5), 1880.

690   54.   Carter, W.; Atkinson, R.; Winer, A.; Pitts, J., Evidence for chamber-dependent radical

691   sources: Impact on kinetic computer models for air pollution. *Int. J. Chem. Kinet.* **1981,** *13*,

692   (8), 735.

693   55.   Akimoto, H.; Takagi, H.; Sakamaki, F., Photoenhancement of the nitrous acid

694   formation in the surface reaction of nitrogen dioxide and water vapor: Extra radical source in

695   smog chamber experiments. *Int. J. Chem. Kinet.* **1987,** *19*, (6), 539.

696   56.   Pereira, K. L.; Hamilton, J. F.; Rickard, A. R.; Bloss, W. J.; Alam, M. S.; Camredon,

697   M.; Muñoz, A.; Vázquez, M.; Borrás, E.; Ródenas, M., Secondary organic aerosol formation

30

698 and composition from the photo-oxidation of methyl chavicol (estragole). *Atmos. Chem.*

699 *Phys.* **2014,** *14*, (11), 5349.

700 57.   Donahue, N.; Robinson, A.; Stanier, C.; Pandis, S., Coupled partitioning, dilution, and

701 chemical aging of semivolatile organics. *Environ. Sci. Technol.* **2006,** *40*, (8), 2635.

702 58.   Stanier, C. O.; Donahue, N.; Pandis, S. N., Parameterization of secondary organic

703 aerosol mass fractions from smog chamber data. *Atmos. Environ.* **2008,** *42*, (10), 2276.

704 59.   Pankow, J. F., An absorption model of the gas/aerosol partitioning involved in the

705 formation of secondary organic aerosol. *Atmos. Environ.* **1994,** *28*, (2), 189.

706 60.   Pankow, J. F., An absorption model of gas/particle partitioning of organic compounds

707 in the atmosphere. *Atmos. Environ.* **1994,** *28*, (2), 185.

708 61.   Jenkin, M. E.; Saunders, S. M.; Pilling, M. J., The tropospheric degradation of volatile

709 organic compounds: A protocol for mechanism development. *Atmos. Environ.* **1997,** *31*, (1),

710 81.

711 62.   Bröske, R.; Kleffmann, J.; Wiesen, P., Heterogeneous conversion of no2 on secondary

712 organic aerosol surfaces: A possible source of nitrous acid (hono) in the atmosphere? *Atmos.*

713 *Chem. Phys.* **2003,** *3*, (3), 469.

714 63.   Bejan, I.; Abd El Aal, Y.; Barnes, I.; Benter, T.; Bohn, B.; Wiesen, P.; Kleffmann, J.,

715 The photolysis of ortho-nitrophenols: A new gas phase source of hono. *PCCP* **2006,** *8*, (17),

716 2028.

717 64.   Kleffmann, J., Daytime sources of nitrous acid (hono) in the atmospheric boundary

718 layer. *J. Chem. Phys. Phys. Chem.* **2007,** *8*, (8), 1137.

31

719   65.   Forstner, H. J. L.; Flagan, R. C.; Seinfeld, J. H., Secondary organic aerosol from the

720   photooxidation of aromatic hydrocarbons: Molecular composition. *Environ. Sci. Technol.*

721   **1997,** *31*, (5), 1345.

722   66.   Jang, M.; Kamens, R. M., Characterization of secondary aerosol from the

723   photooxidation of toluene in the presence of nox and 1-propene. *Environ. Sci. Technol.* **2001,**

724   *35*, (18), 3626.

725   67.   Hamilton, J. F.; Webb, P. J.; Lewis, A. C.; Reviejo, M. M., Quantifying small

726   molecules in secondary organic aerosol formed during the photo-oxidation of toluene with

727   hydroxyl radicals. *Atmos. Environ.* **2005,** *39*, (38), 7263.

728   68.   Sato, K.; Hatakeyama, S.; Imamura, T., Secondary organic aerosol formation during

729   the photooxidation of toluene: Nox dependence of chemical composition. *J. Phys. Chem. A.*

730   **2007,** *111*, (39), 9796.

731   69.   Zhong, M.; Jang, M.; Oliferenko, A.; Pillai, G. G.; Katritzky, A. R., The soa

732   formation model combined with semiempirical quantum chemistry for predicting uv-vis

733   absorption of secondary organic aerosols. *PCCP* **2012,** *14*, (25), 9058.

734   70.   Sato, K.; Takami, A.; Kato, Y.; Seta, T.; Fujitani, Y.; Hikida, T.; Shimono, A.;

735   Imamura, T., Ams and lc/ms analyses of soa from the photooxidation of benzene and 1, 3, 5-

736   trimethylbenzene in the presence of no x: Effects of chemical structure on soa aging. *Atmos.*

737   *Chem. Phys.* **2012,** *12*, (10), 4667.

738   71.   Cabral do Couto, P.; Guedes, R. C.; Costa Cabral, B. J.; Martinho Simões, J. A.,

739   Phenol o–h bond dissociation energy in water clusters. *Int. J. Quantum Chem* **2002,** *86*, (3),

740   297.

741   72.   Parthasarathi, R.; Subramanian, V.; Sathyamurthy, N., Hydrogen bonding in phenol,

742   water, and phenol−water clusters. *J. Phys. Chem. A.* **2005,** *109*, (5), 843.

743   73.   Tsui, H. H. Y.; van Mourik, T., Ab initio calculations on phenol−water. *Chem. Phys.*

744   *Lett.* **2001,** *350*, (5–6), 565.

745   74.   Benoit, D. M.; Clary, D. C., Quantum simulation of phenol−water clusters. *J. Phys.*

746   *Chem. A.* **2000,** *104*, (23), 5590.

747   75.   An, X.; Jing, B.; Li, Q., Regulating function of alkali metal on the strength of oh···o

748   hydrogen bond in phenol–water complex: Weak to strong and strong to weak. *Comp.Theor.*

749   *Chem.* **2011,** *966*, (1–3), 278.

750   76.   Chen, P. C.; Chen, S. C., Theoretical study of the internal rotational barriers in

751   nitrobenzene, 2-nitrotoluene, 2-nitrophenol, and 2-nitroaniline. *Int. J. Quantum Chem* **2001,**

752   *83*, (6), 332.

753   77.   Chen, P. C.; Lo, W.; Tzeng, S. C., Molecular structures of mononitrophenols and their

754   thermal decomposition tautomers. *J. Mol. Struct.* **1998,** *428*, (1–3), 257.

755   78.   Olariu, R. I.; Bejan, I.; Barnes, I.; Klotz, B.; Becker, K. H.; Wirtz, K., Rate

756   coefficients for the gas-phase reaction of no3 radicals with selected dihydroxybenzenes. *Int.*

757   *J. Chem. Kinet.* **2004,** *36*, (11), 577.

758   79.   Bejan, I. G. Investigations on the gas phase atmospheric chemistry of nitrophenols

759   and catechols. Bergische University of Wupperthal, Germany, 2006.

760   80.   Chen, J.; Wenger, J. C.; Venables, D. S., Near-ultraviolet absorption cross sections of

761   nitrophenols and their potential influence on tropospheric oxidation capacity. *J. Phys. Chem.*

762   *A.* **2011,** *115*, (44), 12235.

763   81.   Atkinson, R.; Aschmann, S. M., Products of the gas-phase reactions of aromatic

764   hydrocarbons: Effect of no2 concentration. *Int. J. Chem. Kinet.* **1994,** *26*, (9), 929.

765   82.   Atkinson, R., Atmospheric chemistry of vocs and nox. *Atmos. Environ.* **2000,** *34*, (12-

766   14), 2063.

767   83. Orlando, J. J.; Tyndall, G. S.; Calvert, J. G., Thermal decomposition pathways for

768   peroxyacetyl nitrate (pan): Implications for atmospheric methyl nitrate levels. *Atmos.*

769   *Environ. Part A. General Topics* **1992,** *26*, (17), 3111.

770   84.   Zou, Y.; Deng, X. J.; Zhu, D.; Gong, D. C.; Wang, H.; Li, F.; Tan, H. B.; Deng, T.;

771   Mai, B. R.; Liu, X. T.; Wang, B. G., Characteristics of 1 year of observational data of vocs,

772   nox and o3 at a suburban site in guangzhou, china. *Atmos. Chem. Phys.* **2015,** *15*, (12), 6625.

773   85.   Bloss, C.; Wagner, V.; Jenkin, M. E.; Volkamer, R.; Bloss, W. J.; Lee, J. D.; Heard,

774   D. E.; Wirtz, K.; Martin-Reviejo, M.; Rea, G.; Wenger, J. C.; Pilling, M. J., Development of

775   a detailed chemical mechanism (mcmv3.1) for the atmospheric oxidation of aromatic

776   hydrocarbons. *Atmos. Chem. Phys.* **2005,** *5*, (3), 641.

34

Table 1 - Initial mixing ratios of the oxidants and VOC precursors investigated, including chamber humidity and chamber temperature for the experiments performed during the TOXIC and ATMECH project.

Project	Date	Exp.	Exp. Description	Initial mixing ratio[a]			Oxidant initial mixing ratio[a]			VOC:NO$_x$	Experimental range[b]	
				Toluene [ppbv]	Methyl chavicol [ppbv]	4-Methyl Catechol [ppbv]	NO [ppbv]	NO$_2$ [ppbv]	O$_3$ [ppbv]		RH [%]	Temperature [K]
TOXIC	20.07.09	Tol$_{low}$	Low NO$_x$	535	-	-	41	< LOD	< LOD	~13:1	0.2 – 2.9	297 - 308
	21.07.09	Tol$_{mod}$	Moderate NO$_x$	560	-	-	105	< LOD	< LOD	~5:1	1.1 – 2.1	297 - 309
	28.07.09	4-MCat		-	-	591	120	2	< LOD	~5:1	0.2 – 8.8	298 - 305
ATMECH	15.05.12	MC$_{[high]}$		-	460	-	92	3	5	~5:1	2.1 -10.7	297 - 306

[a] = On the opening of the chamber covers. [b] = From the opening to the closing of the chamber covers.
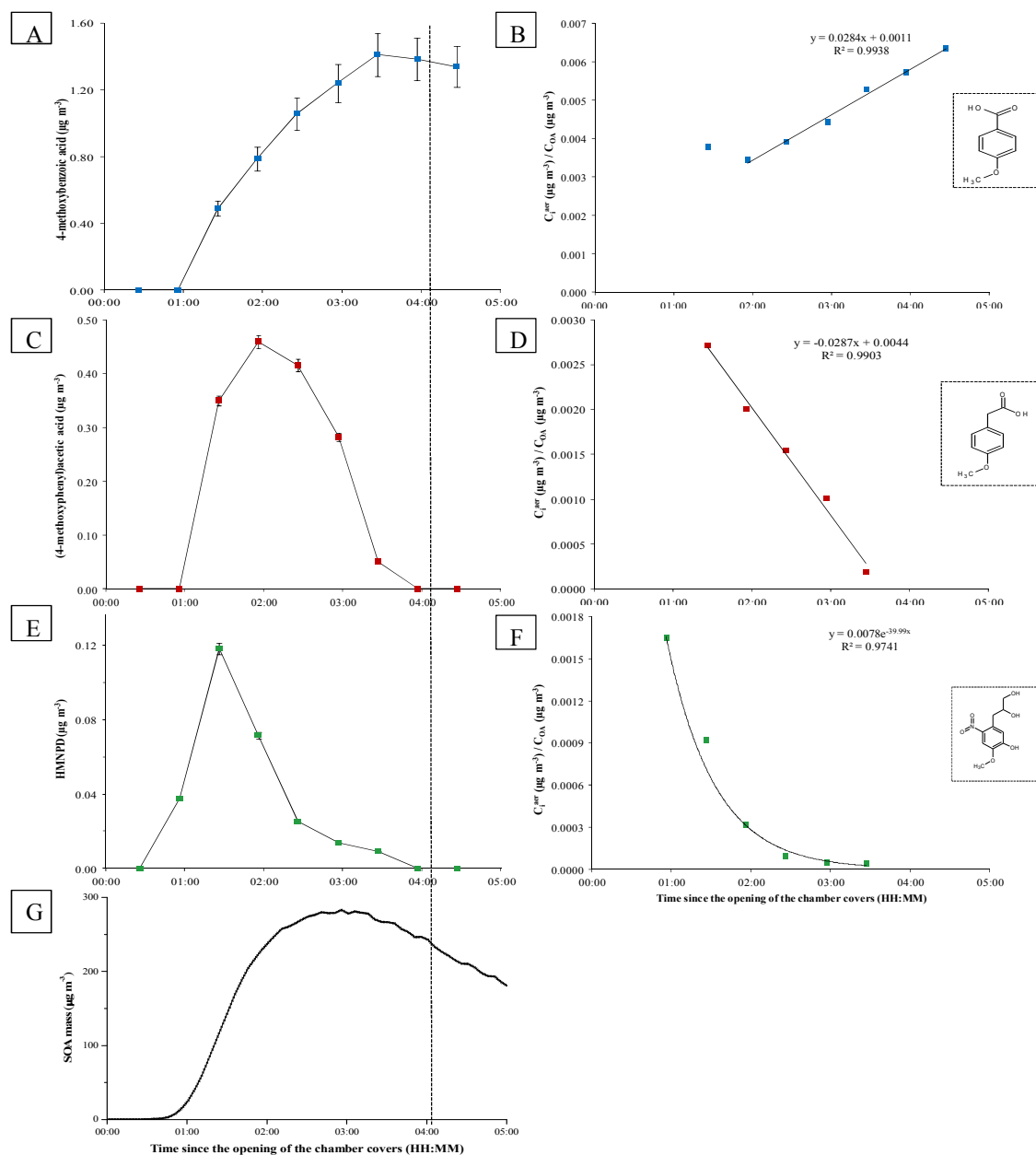
Figure 1 - Types of characteristic particulate phase temporal profile shapes observed in MC$_{[high]}$ (*left*) and their measured mass fraction ($y_i = C_{i,\text{aer}}/C_{OA}$) over time (*right*). A = TP1, 4-methoxybenzoic acid. B = 4-methoxybenzoic acid (µg m^{-3})/ average SOA mass (µg m^{-3}). C = TP2, (4-methoxyphenyl)acetic acid. D = (4-methoxyphenyl)acetic acid (µg m^{-3})/ average SOA mass (µg m^{-3}). E = TP3, HMNPD (3-(5-hydroxy-4-methoxy-2-nitrophenyl)propane-1,2-diol). F = HMNPD (3-(5-hydroxy-4-methoxy-2-nitrophenyl)propane-1,2-diol) (µg m^{-3})/ average SOA mass (µg m^{-3}). G = SOA mass. Compound structures are shown in the boxes.

36

Temporal profiles are plotted using the average PILS sampling time. Error bars display the average %RSD of the calibration graph used to determine the compound concentrations (see SI for further information). Dashed vertical line = closing of the chamber covers.
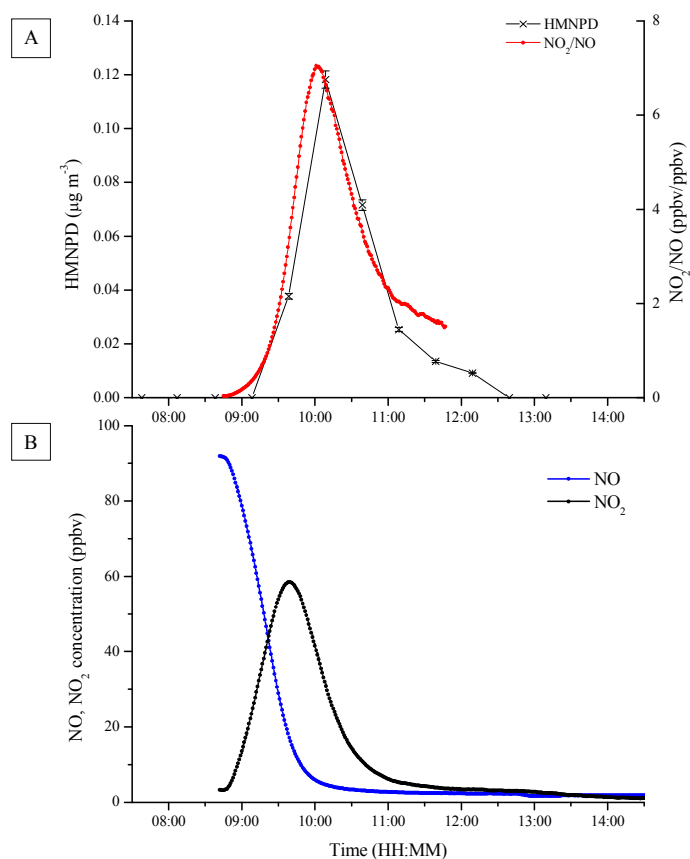

Figure 2 – Temporal profile of the NO_2/NO concentration ratio (ppbv/ppbv) and the particulate phase temporal profile of HMNPD (3-(5-hydroxy-4-methoxy-2-nitrophenyl)propane-1,2-diol, SI compound 1, Table S2) in $MC_{[high]}$. (A) Black = particulate phase temporal evolution of 3-(5-hydroxy-4-methoxy-2-nitrophenyl)propane-1,2-diol. Red = temporal profile of the NO_2/NO ratio (ppbv/ppbv). (B) Blue = NO (ppbv). Black = NO_2 (ppbv).
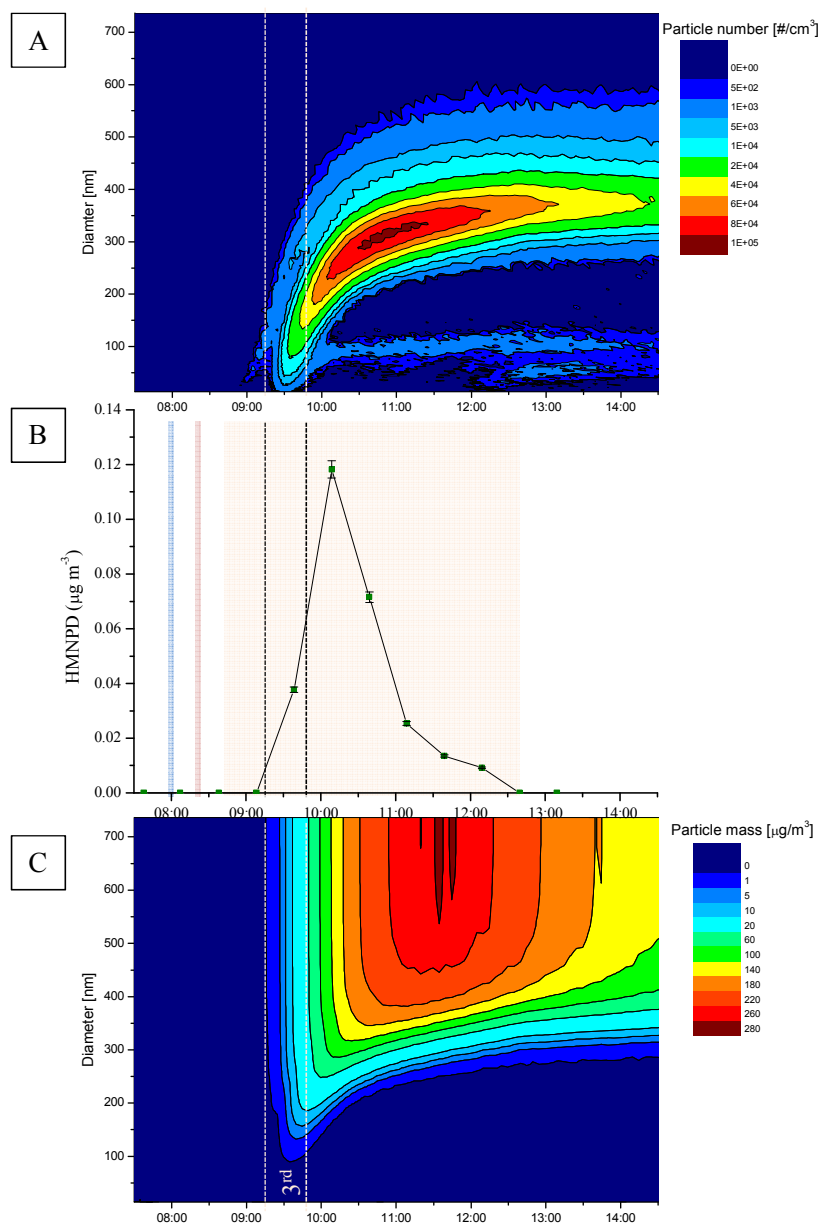
37

Figure 3 - Particle diameter *vs.* time with a coloured contour plot displaying increasing particle number (A) and particle mass (C), compared with the particulate phase temporal profile of HMNPD (3-(5-hydroxy-4-methoxy-2-nitrophenyl)propane-1,2-diol) (B) (SI compound 1, Table S1) during $MC_{[high]}$. Shaded areas in (B); Blue = NO addition. Red = methyl chavicol addition. Orange = opening to the closing of the chamber covers. Dashed lines display the first PILS sampling period where SOA was first observed (3rd sample from the opening of the chamber covers).

38